BIOCHEMISTRY
including biophysical chemistry & molecular biology

ARTICLE

pubs.acs.org/biochemistry

Michler's Hydrol Blue: A Sensitive Probe for Amyloid Fibril Detection

Catherine C. Kitts,* Tamás Beke-Somfai, and Bengt Nordén

Department of Physical Chemistry, Chalmers University of Technology, Kemivägen 10, SE-41296 Göteborg, Sweden

Supporting Information

ABSTRACT: Michler's hydrol blue (MHB) is investigated with respect to photophysical properties in varied solvent environment and when bound to insulin and lysozyme fibrils. The MHB chromophore is shown to act like a molecular rotor and bind well to amyloid fibrils, where it exhibits a characteristic red-shift in its excitation spectrum and an increase in the emission quantum yield upon binding. MHB is more sensitive to environmental changes than Thioflavin T (ThT) and furthermore, in contrast to the latter amyloid probe, can differentiate between insulin and lysozyme fibrils by a more red-shifted excitation spectrum for insulin fibrils. To support the experimental observations, time-dependent density functional theory (TDDFT) calculations were performed on MHB at several levels of theory. The predicted changes of spectral properties as a function of the environment are in good agreement with the experimental results. Linear dichroism (LD) is used to determine the orientation of the MHB within the fibrils. It was shown through LD and molecular modeling that MHB aligns itself preferentially parallel with the amyloid fiber at an angle of 14°−22° to the fibril axis and along the grooves of the β-sheet.

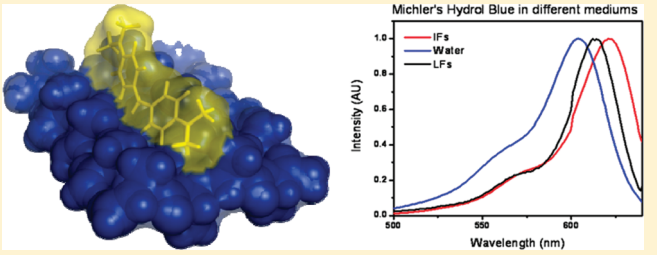

Amyloid fibrils are peptide or polypeptide aggregates that have been extensively studied due to their association with a variety of neurodegenerative diseases, the most famous being Alzheimer's disease.[1−7] Such conformational disorders are caused when native proteins misfold and form self-assembled, insoluble aggregates,[8,9] which accumulate in different organs or tissues. The structure of amyloid fibrils has been found to be composed of antiparallel β-sheets, which are oriented perpendicular to the long fibril axis.[2,3,10−12] The fibrils themselves are nonbranching and can be up to several micrometers long with a width between 8 and 10 nm.[10,12] Although amyloid fibrils are mainly associated with neurodegenerative diseases, other proteins not related to such diseases have been found to form fibrils, too.[2] It is only recently becoming widely accepted that potentially any protein could form amyloid fibrils under specific conditions[13−15] and that fibril formation is an intrinsic property of the polypeptide backbone.[2] Extensive characterization of amyloid fibrils has been made using various spectroscopy and microscopy techniques.[14,16−21]

An often exploited method for spectroscopic determination of amyloid fibril formation is to use one of two histological dyes, Congo Red (CR) or Thioflavin T (ThT). These dyes are of particular interest because of their distinct spectral changes when bound to the amyloid fibrils. CR's absorbance spectrum exhibits a red-shift upon binding[22,23] along with an apple-green birefringence when viewed through crossed polarizers.[23−28] However, CR has been found to not be amyloid specific and can bind to proteins also in their native state.[26] ThT, on the other hand, shows a red-shift in its excitation spectrum[29,30] along with an enhancement in its fluorescence intensity upon binding to fibrils.[13,29−35] In particular, ThT belongs to a class of molecular rotors that have been shown to be sensitive to changes in environmental conditions such as viscosity.[34] Numerous studies have been devoted to the photophysical properties of ThT acting as a molecular rotor in various media as well as bound to amyloid fibrils.[31,34,36−40]

Molecular rotors are particularly interesting for use as amyloid binding agents due to their distinct spectral changes depending on environmental factors and an increase in quantum efficiency upon being geometrically confined.[41] They are comprised of an electron donor system in conjugation with an electron acceptor and connected generally with a single bond. Upon photoexcitation of these molecules, they can enter a fluorescent locally excited state (LE) or then, through internal rotation around the single bond to 90° which breaks the conjugation of the molecule, relax into a nonfluorescent twisted internal charge transfer (TICT) state.[42,43] The interconversion of both these states is dependent on the viscosity of the surrounding environment.[31,34,43,44] In low-viscosity media, the internal rotation of a molecular rotor encounters little hindrance and the main emission pathway is nonradiative. However, increasing the viscosity of the solvent medium hinders the internal rotation, causing the molecule to become more rigid. This prevents the molecule from entering into a TICT state; the molecule then remains in its LE state and loses its energy through radiative decay. This phenomenon is usually observed in the form of an increased fluorescence

Received: December 20, 2010
Revised: March 11, 2011
Published: March 29, 2011

intensity and high quantum yield.[43] These unique properties make molecular rotors attractive as probes for amyloid fibril structure determination. Although, ThT has been used extensively for amyloid fibril characterization, researchers are synthesizing analogues in search for more efficient dyes that can be used for in vitro and in vivo imaging, in particular dyes that may cross the blood brain barrier.[27]

One particular molecular rotor that in preliminary studies has shown promise as an amyloid fibril binding analogue is Michler's hydrol blue (MHB). Although MHB has been known for over 50 years it has not been used for amyloid fibril detection, probably because of the popularity of ThT, CR, and their analogues. MHB is a small, symmetric molecule that has two dimethylaminophenyl groups attached to a central carbon atom with a positive charge. MHB is related to triphenylmethane dyes like Crystal Violet and Methyl Green, both of which have been found to bind to amyloid fibrils (unpublished results). Theoretical calculations have shown that MHB is a nearly planar molecule with its positive charge delocalized over the entire π-system.[42,45] However, the conjugation can be broken upon the rotation of one of its phenyl rings around the central carbon atom to a 90° geometry relative to the other ring. MHB's size, similar in length to ThT and amino groups at the ends, makes it an ideal candidate for amyloid fibril detection.

In this paper, we will demonstrate that MHB is indeed an excellent amyloid fibril probe. The photophysical properties of MHB, alone in solution and in the presence of amyloid fibrils, will be discussed against theoretical calculations that plot ground and excited state energy barriers as a function of rotation of phenyl rings and in different environments. In addition, to interpret the experimentally observed spectral changes, sheet models with bound MHB are built and optimized using ONIOM[46] calculations with a dispersion-corrected density functional, in order to estimate how the MHB molecule is incorporated into the amyloid β-sheet. The optical properties of MHB as a molecular rotor were explored in various ethanol/glycerol solutions ranging from low to high viscosity with absorbance and fluorescence spectroscopy. Absorbance and fluorescence spectroscopy were also used to probe MHB free in solution and in the presence of amyloid fibrils made from insulin or lysozyme. Upon binding, MHB, a molecular rotor that has its internal rotation restricted, should exhibit a red-shift in absorbance spectrum and an increase in quantum efficiency.

Flow linear dichroism (LD) was also used to determine MHB's orientation within the amyloid fibrils. LD is a differential polarized-light absorption spectroscopy technique that exploits a Couette flow cell to align macromolecules parallel to the flow direction,[47,48] and previous studies have shown that the fibrils can easily be oriented this way.[49−51] The sample is illuminated with light polarized in the vertical ($A_{\parallel}$) and horizontal direction ($A_{\perp}$) with respect to the sample orientation. The LD is then calculated by subtracting the perpendicular absorbance from the parallel absorbance:

$$\mathrm{LD} = A_{\parallel} - A_{\perp} \quad (1)$$

The resulting LD spectrum gives structural information on how the fibrils are oriented and about any associated molecules, such as MHB. The fibrils being long filaments can be easily aligned in the flow direction. Insulin was the main protein used in this study because it is well characterized, readily forms amyloid fibrils, and only has one aromatic amino acid, tyrosine, which absorbs light in the UV region. Another protein, lysozyme, was used for comparison.

EXPERIMENTAL PROCEDURES

Materials. Michler's hydrol blue (MHB) was a gift from the late Dr. Gösta Bengtsson, University of Lund (for synthesis see ref 52), and its purity was confirmed by ^{1}H NMR and GC−mass spectrometry. Thioflavin T (ThT), insulin from bovine pancreas, lysozyme from chicken egg white, and glycerol were used as purchased from Sigma-Aldrich with no further purification.

Insulin fibrils and lysozyme fibrils were prepared by dissolving the protein in pH 2 water (0.01 M HCl) (5 mg/mL for insulin and 10 mg/mL for lysozyme). The solutions were filtered through a 0.2 μm filter. Insulin fibril solutions were heated at 60 °C for 24 h, while lysozyme fibril solutions were heated at 60 °C for 6 days. After heating, the solutions were cooled and then centrifuged (Jouan SA A14 centrifuge) at 3000 rpm for 3 min to remove any globular particulates. The supernatant liquid containing the fibrils was removed and stored at 10 °C until needed; this was used as the stock fibril solution. Fibril solutions were not used past 1 week.

Michler's hydrol blue stock solution was made by dissolving MHB in a 10 mM citrate buffer (pH 4) to a concentration of 0.8 mg/mL (1.134 mM). Solutions for absorbance and fluorescence spectroscopy containing only MHB were made by diluting an aliquot of MHB stock solution with pH 4 buffer to give the desired concentration. Solutions containing insulin or lysozyme fibrils and MHB were prepared by diluting 100 μL of the stock fibril solution and an aliquot of the MHB stock solution with pH 4 buffer. A solution composed of insulin (5 mg/mL) or lysozyme (10 mg/mL) protein in pH 2 water was also prepared, but not fibrillized. An aliquot of this solution was combined with a portion of the MHB stock solution and diluted with pH 4 buffer solution to yield the same MHB concentration as above. ThT stock solution was made by dissolving ThT in Milli-Q water to give a concentration of 0.8 mg/mL (2.5 mM). ThT solutions alone and with fibrils were prepared in a similar fashion as above. Solutions used for viscosity studies were prepared in the following way. MHB was dissolved in ethanol (0.4 mg/mL) to use as a stock solution. An aliquot of the MHB stock solution in ethanol was dissolved in solutions with different ratios of EtOH:glycerol (100:0, 80:20, 50:50, 40:60, 30:70, 20:80, 10:90, 6:94), while maintaining a constant MHB concentration. Solutions used for LD were made by diluting a portion of the stock fibril solution and an aliquot of 0.8 mg/mL MHB in pH 4 buffer with additional buffer to a final volume of 1.80 mL; LD solutions containing ThT were made in a similar fashion, but diluted with pH 5 citrate buffer.

Methods. Absorbance spectra were collected on a Varian Cary 4000 UV−vis spectrophotometer. Spectra were collected using a 1.4 mL volume Hellma quartz cuvette with a path length of 1 cm, except for the linear dichroism solutions, which absorbance spectra were collected using a cuvette with a path length of 0.1 cm (same path length as Couette cell). Excitation and emission spectra were collected on a Jobin Yvon-Spex Fluorolog fluorometer.

Time-resolved emission measurements were performed using a pulsed LED (600 nm) from PicoQuant as excitation source, with a PDL 800-B driver operated at 10 MHz. The pulse width of the LED is ≈1 ns. The emission polarizer was set at magic angle, and the light was detected perpendicular to the excitation source,

Scheme 1. Michler's Hydrol Blue and Dihedral Angles φ and φ'

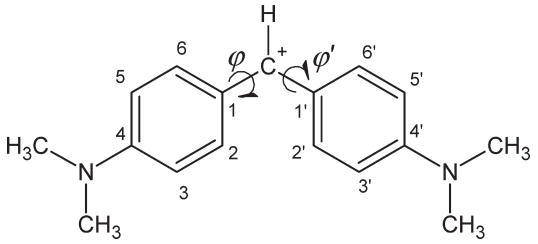

using a monochromator and a LifeSpec II detection system from Edinburgh instruments. The monochromator was set to the maximum emission wavelength. The iris was used to adjust the number of counts to never exceed 10 000 cps.

Linear dichroism (LD) spectra were collected on an Applied Photo Physics Chirascan in LD mode, using a quartz Couette flow cell with path length of 0.1 cm. LD samples were ultracentrifuged using a Beckman LE 80 ultracentrifuge.

The calculations were performed using the Gaussian 09 software package.[53] Excited state energies as well as UV-vis spectra were calculated using time-dependent density functional theory (TDDFT), which can accurately determine spectral properties of larger organic dyes[54] at a relatively low computational cost[55] by using the B3LYP functional[56,57] and a medium-sized basis set, 6-31+G(d). Unfortunately, for MHB and similar cationic cyanine and polymethine dyes, TDDFT shows a systematic error by overestimating excitation energies, which results in markedly shorter absorption wavelengths than obtained by experimental measurements.[55,58,59] However, because of the systematic nature of the latter error, the relative effects of various solvents can be accurately characterized. Thus, solvent effects of water, ethanol, and glycol were considered by using the integral equation formalism polarizable continuum solvent model (IEFPCM),[60] as implemented in Gaussian 09. Glycol was compared to the experimental shifts observed in glycerol as parameters for the latter solvent are not implemented in the used software package. To estimate the Boltzmann distribution of the different conformations of MHB and its effect on excitation wavelength, a stepwise geometry scan was performed along φ (2-1-C^+-1′) in the range of 0−180° with 10° resolution at the B3LYP/6-31G level of theory (Scheme 1). This resulted in a full rotation of the two aromatic planes with respect to each other. The obtained structures were submitted to TDDFT calculations at the TDDFT (B3LYP)/6-31+G(d) level of theory. To model MHB bound on the sheet surface formed by the amyloid fibrils, a five-stranded antiparallel sheet model, $[HCO\text{-}Ala_5\text{-}NH_2]_5$, was obtained based on structures reported by Perczel et al.[61] (Figure S4). The orientation of MHB was based on previously reported dye−fibril interactions by using molecular dynamics simulations[62,63] with using ThT as the dye molecule. Final optimization on the position of MHB on the sheet model with two possible orientations was performed by using a two-layered ONIOM setup, ωB97X-D/6-31G(d):PM3, with MHB and the closer residues on the sheet in the high layer. The optimized geometries were submitted to TDDFT calculations with an ONIOM-TDDFT(B3LYP/6-31+G(d)):PM3 setup using the IEFPCM model to represent the aqueous environment. Recently, several new functionals were considered to be superior with lower deviation from experimental values over the standard B3LYP functional.[64,65] To validate these for MHB, we performed TDDFT calculations using several functionals with different basis sets, which showed excellent correlation with those obtained by B3LYP/6-31+G(d), thus confirming our method of choice for MHB. For more computational details, setup of the ONIOM layers, and reference calculations on the protein models with ThT, see the Supporting Information.

RESULTS AND DISCUSSION

MHB Spectral Properties. Michler's hydrol blue (MHB) belongs to a class of dyes that behave as molecular rotors, and as such its photophysical properties were explored as a function of polarity and viscosity. Molecular rotors are very sensitive to changes in viscosity that hinders rotation around the central atom. Therefore, solutions containing varying amounts of ethanol and glycerol were used to demonstrate how viscosity affects MHB's spectral properties. The concentration of glycerol was varied from 0% glycerol (100% ethanol) to 94% glycerol (6% ethanol), and absorbance and emission spectra were collected for each solution. Figure 1A shows the normalized absorbance spectra for each of the ethanol:glycerol solutions. The absorbance spectra show a clear red-shift with increasing glycerol concentration and decrease in polarity. When the absorbance maximum is plotted versus percent glycerol, the graph shows a linear characteristic with increasing viscosity/decrease in polarity. The reason for the blue-shift with increasing polarity is due to the stabilization of the ground state by the polar solvents. In MHB, the positive charge is evenly distributed over the molecule, and polar solvents stabilize this localization, leading to the observed blue-shift. However, with more nonpolar solvents, this stabilization is reduced leading to a red-shift in the absorbance spectrum. The emission spectra of MHB in the same solutions show an exponential increase in fluorescence intensity with increasing viscosity (Figure 1B). The low quantum efficiency of MHB in 100% EtOH is an effect of the torsional relaxation of the molecule in the excited state. Upon excitation in EtOH, MHB goes from a locally excited state to a nonfluorescent TICT state upon internal rotation around the central carbon by one of the phenyl rings. The TICT state geometry is 90° relative to the two rings, which is the lowest energy in the excited state, thus breaking the conjugation of the ring system and giving off its energy in the form of nonradiative decay. This internal rotation is much faster than the fluorescence decay, which is why MHB free in solution has such a weak fluorescence signal. However, upon increasing the viscosity of the solution, MHB's rotation becomes restricted to the ground state planar conformation, and no internal rotation is possible. Therefore, when MHB is in a high-viscosity solvent, it cannot relax into the TICT state but remains in the LE state and gives off its energy in the form of fluorescence. This accounts for the increase in the quantum efficiency of MHB with increase in viscosity.

Michler's hydrol blue was studied using absorption and fluorescence spectroscopy in order to determine whether MHB would bind to amyloid fibrils and characterize its spectral properties. Since MHB behaves as a molecular rotor, it is expected that, upon confinement in the fibrils, distinct spectral changes should be observed similar to those with thioflavin T (ThT). Absorption, emission, and excitation spectra were taken of MHB alone in pH 4 buffer. Figure 2 shows the normalized absorbance and emission spectra (red lines). The absorption of

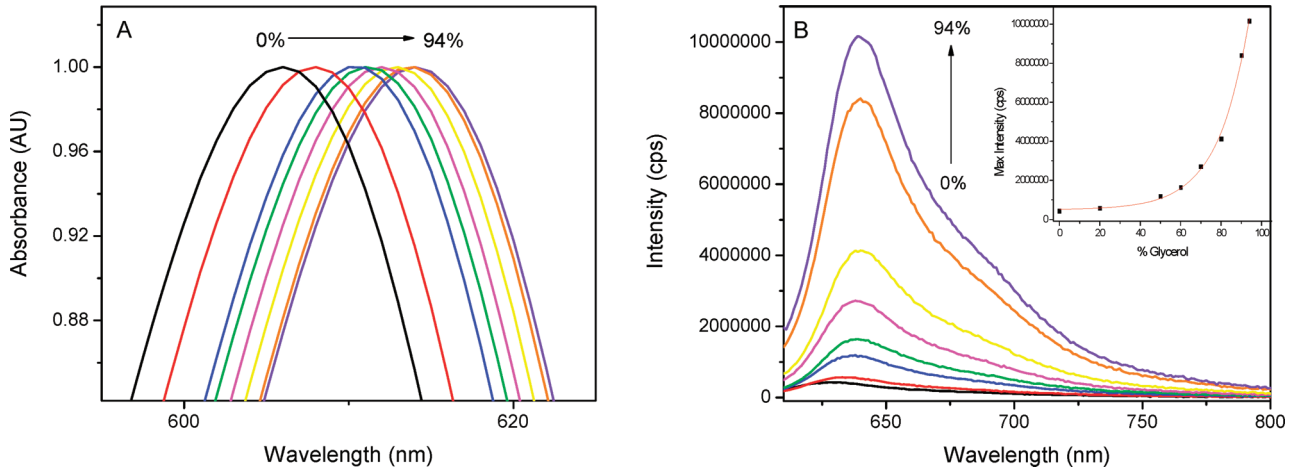

Figure 1. (A) Normalized absorbance spectra of MHB in different ratios of ethanol:glycerol (only the top section of the peaks are shown). (B) Emission spectra of MHB in different ratios of ethanol:glycerol. 100:0 (black), 80:20 (red), 50:50 (blue), 40:60 (green), 30:70 (magenta), 20:80 (yellow), 10:90 (orange), and 6:94 (violet). Inset: plot of the emission intensity for each solution versus percentage glycerol present.

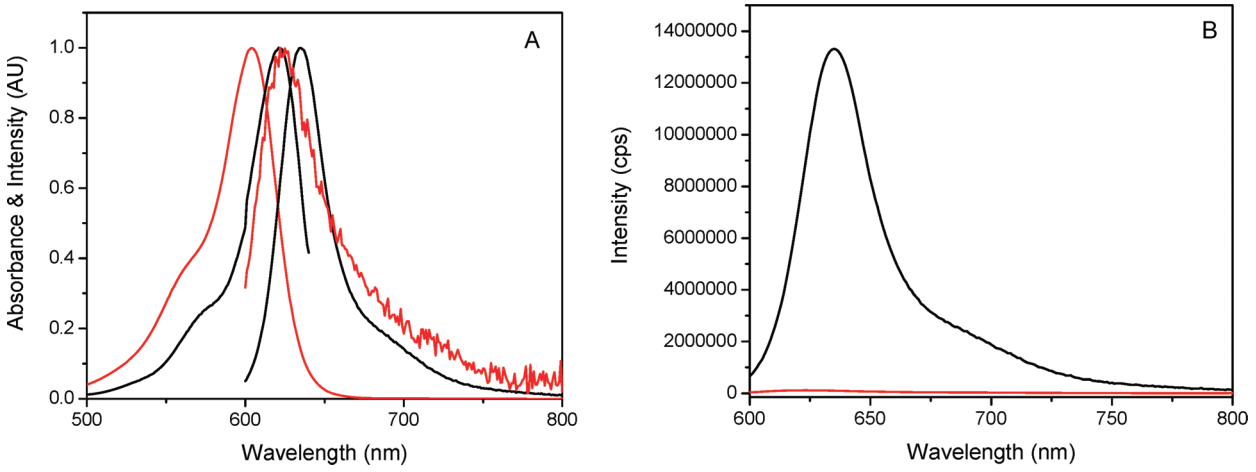

Figure 2. (A) Normalized absorbance and emission spectra of MHB alone in solution (red) and the normalized excitation and emission spectra of MHB bound to insulin fibrils (black). (B) Original emission spectra of MHB alone (red) and bound (black).

MHB alone in pH 4 buffer had a maximum peak at 605 nm with a small shoulder at ~560 nm. The fluorescence emission spectrum, acquired with an excitation of 590 nm, showed a single peak at ~625 nm. The excitation spectrum had a similar shape to the absorbance spectrum with maximum at 605 nm as well (data not shown). When insulin fibrils were introduced into the solution with MHB, distinct spectral changes were observed. Figure 2 (black lines) shows the normalized spectra of MHB in the presence of insulin fibrils. When the spectra of MHB alone in solution were compared with the spectra of MHB in the presence of insulin fibrils, a dramatic difference was observed (Figure 2). First, there is a distinct red-shift to 623 nm in the excitation spectrum when MHB is in the presence of fibrils. Second, the normalized emission spectra show only a slight red-shift to 637 nm; however, when the two un-normalized spectra were compared, a significant increase in the fluorescence intensity was observed. The fluorescence intensity for MHB in the presence of insulin fibrils was ~2 orders of magnitude more fluorescent than when MHB was alone in solution (Figure 2B). These distinct spectral changes indicate that MHB binds to the insulin fibrils much in the same way as ThT dye. To ensure that MHB is binding specifically to insulin fibrils and not to the native protein, absorbance and fluorescence spectra were collected for MHB solutions containing insulin in its native confirmation (data not shown). There was no difference in the spectra containing MHB alone and when native insulin was present; thus, it was concluded that MHB binds specifically to the β-sheet structure of the amyloid fibrils. This behavior of a red-shift in the excitation spectrum and an increase in the quantum efficiency of MHB when bound to fibrils is classic behavior of MHB acting as a molecular rotor.

The differences in the excitation spectrum from the free MHB to the bound MHB are reflected in the change of polarity between the two systems. As discussed above, this blue-shift with increasing polarity is associated with the stabilization of the ground state by polar solvents. When bound to the amyloid fibrils, the MHB experiences a more rigid, nonpolar environment than when free in water. In the emission spectrum, MHB has only a very small change in the emission peaks upon binding to the fibrils. However, the largest difference is in the emission intensity upon incorporation MHB into the fibrils. The increase in fluorescence intensity corresponds with the restriction of the

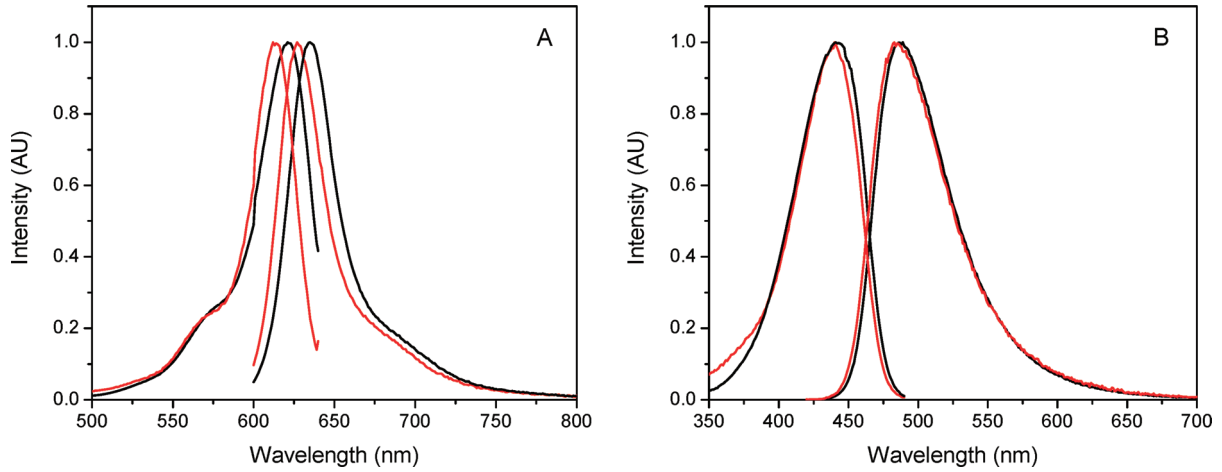

Figure 3. (A) Normalized excitation and emission of MHB bound to insulin fibrils (black) and lysozyme fibrils (red). (B) Normalized excitation and emission of ThT bound to insulin fibrils (black) and lysozyme fibrils (red).

MHB's internal rotation. When MHB is confined to the fibrils, its internal rotation becomes hindered and it cannot relax to the TICT state, but instead remains in the LE state. The characteristic increase in fluorescence intensity when MHB is bound to amyloid fibrils is similar to that of when MHB is in a high-viscosity solvent, which shows that the increase in fluorescence intensity is due to the restricted internal rotation of the MHB. This accounts for the significant increase in quantum efficiency of MHB upon binding to the amyloid fibrils. Michler's hydrol blue's behavior when bound to amyloid fibrils shows similar spectral changes as the extensively studied ThT.

Michler's hydrol blue was also investigated in the presence of lysozyme amyloid fibrils. Absorption, excitation, and emission spectra were collected when MHB was in the presence of lysozyme fibrils (Figure 3A, red lines). MHB exhibited the same spectral behavior as when bound to insulin amyloid fibrils: red-shift in the excitation spectrum and increase in fluorescence intensity. However, when the excitation and emission spectra were compared between MHB bound to insulin fibrils and lysozyme fibrils, differences between the spectra were observed (Figure 3A). The excitation spectrum of MHB bound to lysozyme fibrils was blue-shifted to 615 nm relative to the excitation maximum of MHB bound to insulin fibrils (λ_{max} = 623 nm). The emission maximum is also blue-shifted to 630 nm from that of MHB bound to insulin fibrils (λ_{max} = 637 nm). As discussed above, MHB is sensitive to different environments, where its absorption maximum red-shifts with decreasing polarity. Since MHB's excitation spectrum differs between lysozyme fibrils and insulin fibrils, this would indicate that the environment MHB experiences are different between the two fibrils. This suggests that where MHB binds on insulin fibrils is a more nonpolar environment than where MHB binds on the lysozyme fibrils, which is mostly likely due to the displacement of water molecules upon binding. In order to determine if MHB's sensitivity to the different fibrils was unique to this dye, excitation and emission spectra were taken of ThT bound to insulin fibrils and lysozyme fibrils to see if it also had spectral shifts between the two fibrils. The excitation and emission spectra shown in Figure 3B showed no spectral shifts between the two different fibrils. Thus, while ThT cannot distinguish between lysozyme fibrils and insulin fibrils, we conclude that MHB is a much more sensitive dye to environmental changes even between different amyloid fibrils, making MHB a better dye to use for characterization of amyloid fibrils.

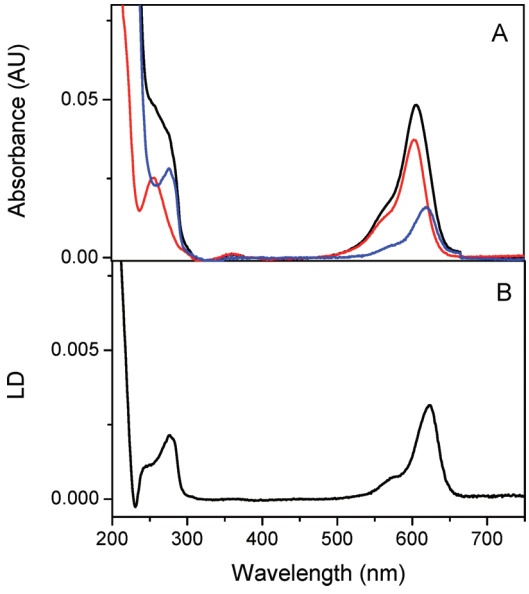

Figure 4. (A) Corresponding absorption spectra of the original MHB−insulin fibril solution (black), after solution was ultracentrifuged (red), and resultant spectrum when supernatant spectrum subtracted from the original spectrum resulting in the absorbance spectrum of bound MHB (blue). (B) Linear dichroism spectrum of MHB bound to insulin fibrils.

Lifetime data were also collected for MHB in insulin fibrils and lysozyme fibrils. The time-resolved fluorescence decays of MHB bound to insulin fibrils and lysozyme fibrils were both represented by a double-exponential fit (Figure S1). The MHB bound to insulin fibrils had a lifetime of 0.31 ns (A_1 = 0.89) and a slower component with a lifetime of 1.11 ns (A_2 = 1.00), while the lifetime of MHB bound to lysozyme fibrils had a lifetime of 0.32 ns (A_1 = 0.87) and a slower component with a lifetime of 1.28 ns (A_2 = 1.00). The lifetime of MHB in glycerol was also collected and had a faster lifetime than MHB bound to fibrils; however, the lifetimes could not be calculated accurately because the IRF was approximately the same width as the lifetime of MHB in glycerol

dx.doi.org/10.1021/bi102016p |*Biochemistry* 2011, 50, 3451–3461

Scheme 2. Transition Moments of Tyrosine

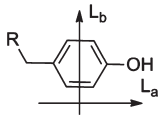

and could not be convoluted with sufficient accuracy. The increase of MHB's lifetime from when it is in glycerol to being bound to the fibrils is indicative of MHB being in a more rigid environment. The increase in the rigidity of the environment leads to a decrease in the nonradiative decay rate, which results in a longer lifetime and higher quantum yield. Although the lifetimes between the two different fibrils did not show a significant difference, the data do give information on the decay rate of MHB when bound.

MHB Orientation within the Fibrils. Linear dichroism (LD) was used to determine MHB's orientation within the fibrils. Once the fibrils are oriented in the flow, absorbance spectra using linearly polarized light in the parallel and perpendicular directions are taken and then subtracted from one another in order to obtain the LD spectra (eq 1). On the basis of the sign and strength of the resulting peaks, one may determine the orientation within the fibrils. A positive peak would indicate that MHB transition moment's long axis is preferentially parallel to the fibril axis, while a negative peak would indicate that MHB is more perpendicular to the fibril axis. Figure 4B is the LD spectrum of MHB bound to insulin fibrils in pH 4 buffer. In the LD spectrum there is a negative peak at 230 nm (L_a) and a positive peak at 276 nm (L_b); these peaks correspond to the orthogonal transitions of tyrosine (Scheme 2). The positive peak at 623 nm corresponds to MHB bound to the insulin fibrils. Since the peak at 623 nm is positive, this indicates that MHB aligns its long axis preferentially parallel to the fibril axis. The reduced LD (LD^r) can then be calculated in order to quantitatively determine MHB's orientation within the fibrils using the following equation:

$$LD^r = \frac{LD}{A_{iso}} = \frac{3}{2}S(3\cos^2\alpha - 1) \qquad (2)$$

where A_{iso} is the absorption of the isotropic solution, S is the orientation factor (this describes how the sample is oriented and may take values between 0 and 1, $S = 1$ corresponding to a perfectly oriented sample), and α is the angle between the dye transition moment and the amyloid fibril axis. The A_{iso} was determined by collecting the absorption spectrum of the LD solution in a 0.1 cm path length cuvette (which is the same path length as the Couette cell used), followed by ultracentrifuging the LD solution in order to pellet the fibrils. The supernatant was then removed, and an absorption spectrum was collected. When the absorption spectrum of the supernatant was subtracted from the original absorption spectrum of the LD solution, the resulting absorption spectrum was that of the MHB bound to amyloid fibrils (Figure 4A). The absorption at 623 nm of the subtracted spectrum was used as the A_{iso} in eq 2 in order to calculate the LD^r of MHB bound. The LD^r (at maximum 623 nm) of MHB bound to insulin fibrils was calculated to be 0.20 at pH 4. A major problem in calculating the angle of MHB within the fibrils is determining the S factor of the fibrils, which can vary depending on the solvent environment and pH. A nonempirical method for rigid rod-shaped particles in Couette flow[66] was first applied, but

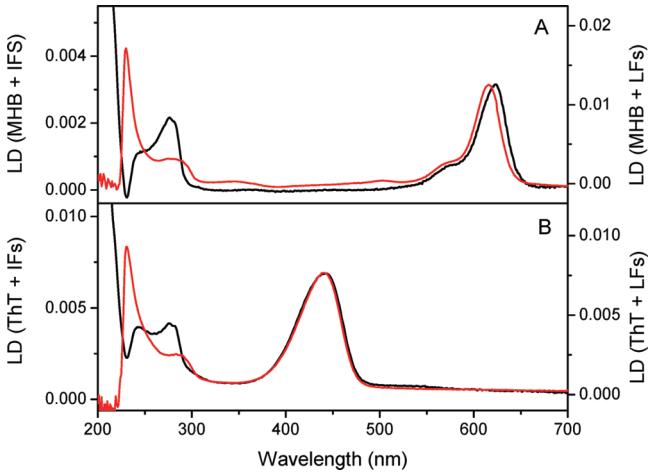

Figure 5. (A) LD spectra of MHB bound to insulin (black) and lysozyme (red) fibrils. (B) LD spectra of ThT bound to insulin (black) and lysozyme (red) fibrils.

the S values calculated for the amyloid fibrils were found to be unphysically high (see Supporting Information for detailed calculations).

Therefore, in order to determine the S factor of the insulin fibrils in an empirical way, ThT was instead used as an internal standard to gauge the S factor of the fibrils. In a near-field optical microscopy study, it was reported that ThT was aligned parallel to the fibril axis and had an upper angle limit of 16°.[67] Thus, using 16° as a reference angle of ThT, a series of LD experiments were performed to determine the S factor of the fibrils and then to calculate the angle of MHB. Four LD samples were prepared at pH 4: (1) Solution containing only insulin fibrils, (2) solution containing insulin fibrils and ThT, (3) solution containing insulin fibrils and MHB, and (4) solution containing insulin fibrils, ThT, and MHB. From the LD spectrum of insulin fibrils and ThT, the S factor was calculated using eq 2, with the LD^r of ThT and α set at 16°. This S factor was then used to calculate the L_b transition angle of the tyrosines in the insulin fibril, which was found to be ~42°. The angle of the L_a transition was not calculated because the LD^r of this transition was too low due to the A_{iso} at 230 nm not only being the absorption of the L_a transition, but also including contributions from other absorbing species. It was then assumed that the tyrosine angles should be fixed within the fibrils so the average angle could be treated as a constant. Using this assumption, the angle of 42° for the L_b transition (276 nm) was used to calculate the S factor of the fibrils, which in turn could then be used to calculate the angle of MHB. The S was inserted into eq 2 along with the LD^r of MHB: $LD^r = 0.20$ and $S = 0.08$, which gives a calculated angle of 22° for MHB. The solution containing insulin fibrils, ThT, and MHB was used to check reproducibility, and it was found that with both dyes present the angles for the tyrosine's L_b transition and MHB angle are consistent. However, as stated previously, 16° was considered the upper limit angle of ThT: if we instead use 0° as the lower limit for ThT's angle and recalculate the L_b transition angle of tyrosine and MHB's angle using the same method as just described, then the L_b transition angle was 40° and MHB's transition angle becomes 14°. This shows that even if ThT's angle varies between 0° and 16°, the resulting MHB angle is affected as well but remains within a reasonable limit. An angular range of 14°−22° is a reasonable range for the MHB's transition

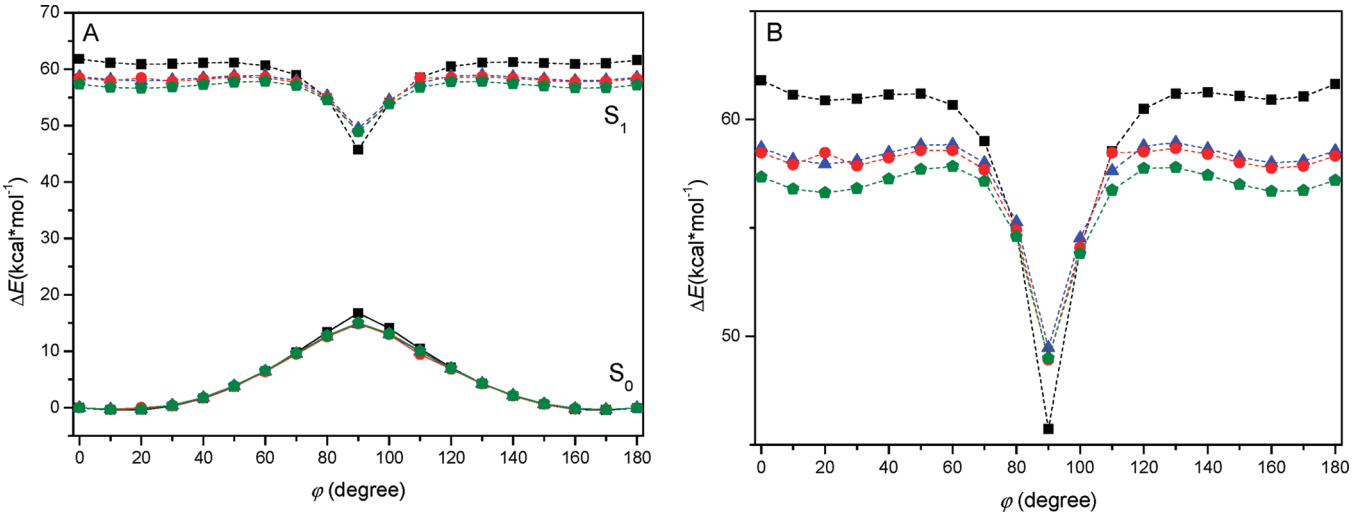

Figure 6. Energies calculated for Michler's hydrol blue in ground S_0 and first excited state S_1 as a function of dihedral angle φ (second angle, $\varphi' = 0$; see Scheme 1) and molecular environment. (A) Relative energy difference between S_0 and S_1 states. (B) Stabilization effect of the investigated solvents on the S_1 state: gas (black squares), water (blue triangles), ethanol (red circles), glycol (olive pentagons).

moment within the fibrils because MHB is a bent molecule and most likely will not sit in the β-sheet grooves with its transition dipole moment perfectly parallel to the fibril axis, but at an angle. Therefore, we conclude that the MHB molecules also align in the β-sheet grooves parallel to the fibril axis, like the ThT dye does.[13,67]

Linear dichroism was also used to investigate MHB's binding to lysozyme fibrils. An LD spectrum for MHB bound to lysozyme fibrils is shown in Figure 5A (red line). The spectrum shows a positive peak at 280 nm, which is the protein peak, and another positive peak at 616 nm, which corresponds to the bound MHB. The angle of MHB bound to lysozyme fibrils could not be calculated due to the spectral overlap of the tyrosines and tryptophans in its amino acid sequence. This means that the angles of tyrosine and tryptophan could not be determined and in turn nor could the *S* factor be determined or the angle of MHB. However, the LD spectra of MHB bound to insulin fibrils and MHB bound to lysozyme fibrils can be compared. When the spectra are overlaid, there is a red-shift in the MHB peak when bound to insulin fibrils. This corresponds exactly to that observed in the excitation spectra, suggesting that the insulin fibrils have a less polar environment to which MHB binds. The LD spectra of ThT bound to insulin fibrils and lysozyme fibrils were also compared (Figure 5B). Again, there was no shift in the ThT peak when bound to the two different fibrils. This observation validates what was observed in the excitation spectra and that MHB is indeed sensitive to differences between amyloid fibrils.

THEORETICAL CALCULATIONS

Precision and Accuracy. To investigate which theoretical methods should be optimal for our current investigation, we compared the $S_0 \rightarrow S_1$ excitation energies obtained at different levels of theory on a single optimized conformation of MHB. Further on, we also investigated the effect of the solvent environment using water, ethanol, and glycol (Table S2). In principle, as already mentioned, accurate calculation of excitation energies is still problematic for charged cyanine dyes, as all investigated methods show a considerable overestimation for the $S_0 \rightarrow S_1$ excitation energies by ~0.43−0.63 eV. In our current investigation, the TDDFT calculations using the B3LYP hybrid functional with a middle size basis set on a geometry obtained with a double-ζ quality basis set show the smallest deviation from experimental shifts. More importantly, when comparing effects of the investigated solvents, all methods show qualitatively similar wavelength shifts as observed experimentally. Thus, for our further calculations the B3LYP/6-31+G(d)//B3LYP/6-31G level of theory was chosen to be the optimal level of approach.

Dihedral Angle Dependence on Excitation. The dependence of the excitation energy on dihedral φ was calculated by a stepwise scan of the intermolecular rotation along the φ torsional angle. This shows that the low-energy region for ground state, S_0, is φ = ~0°−30° and ~150°−180°, where the molecule has a slightly skewed or gauche orientation between the two aromatic rings. In the low-energy conformations the relative energy difference between the ground and singlet excited states is high as it is above 55 kcal/mol (Figure 6A), having extensive conjugation both in the HOMO and LUMO states (Figure S3). When φ is close to 90°, the relative energy of the ground state increases significantly and is accompanied by a decrease in the energy of the S_1 state. At φ = 90° the energy gap between the S_0 and the S_1 states is only ~30 kcal/mol. This is accompanied by a severely reduced conjugation in the HOMO and LUMO states (Figure S3). As expected, the character of the potential energy curve in the S_1 state indicates that the lack of fluorescence in the aqueous phase is due to an internal rotation to the conformation with lowest S_1 energy, where a nonradiative decay takes place, similarly as observed in other analogous molecular rotors.[34]

To characterize the effect of the different environments as well as to support interpretation of the experimental results, the points obtained for all conformations along the above scan were also submitted to TDDFT calculations using water, ethanol, and glycol continuum models (IEFPCM) as a surrounding matrix. In general, when the environment is changed from the gas phase to solvent phase, a relative stabilization of the S_1 can be observed (Figure 6A, Table S2). As mentioned above, the calculated absolute wavelengths are more than 100 nm away from those

obtained experimentally; however, the relative shifts caused by the different surrounding matrix are qualitatively reproduced for the lowest energy conformer. The obtained conformations along the scan of the dihedral angle φ allow us to consider the Boltzmann distribution of them, which should result an average excitation energy calculated in a particular solvent. When comparing the relative wavelength shifts with considering the Boltzmann distribution of the conformations along the scan of φ and their average excitation energies, the shifts caused by the different surrounding matrix are rather accurately reproduced (Table 1).

The theoretical description of MHB bound to the fibrils was obtained using an antiparallel β-sheet model which was based on previous MD simulations and X-ray crystal analysis of ThT binding to amyloid fibrils (for details see Methods and Supporting Information).[63] Accordingly, the dye molecules bind to the amyloid fibrils with their transition moments' long axis oriented parallel to the fibril axis, which is also supported by the current LD spectra of MHB and previous studies.[13,67] The sheet model representing a fragment of the amyloid fibril was composed of 5 strands with a total of 20 alanine residues. Positioning of MHB was considered with two possible orientations on the sheet model: one with its C+ atom closer to the sheet (*C*) (Figure 7) and one with C+ pointing away from the sheet (*A*) (Figure S4B). Optimization of *C* and *A* orientations were obtained by applying a two-layered ONIOM setup (ωB97X-D/6-31G:PM3), in which MHB and the surrounding residues were calculated with the ωB97X-D functional which has a damped atom−atom dispersion correction included.[68] Considering structural properties of the bound MHB, both *C* and *A* have its long axis nearly parallel to the sheet plane, with *C* being somewhat more tilted along its long axis with respect to the sheet plane than *A*. As in the case of the single optimized conformation of MHB calculated with implicit solvent models of water, ethanol, and glycol (Table 1), the sheet model *C* and *A* and the applied theoretical approaches include the main characteristics of a β-sheet fragment and the positioning of MHB on the sheet surface. Thus, these are feasible to qualitatively describe environmental changes around the MHB molecule when they are bound to the fibrils with a certain orientation. The experimental absorption peak at 604 nm in water shows a ~19 nm red-shift when MHB is bound to insulin fibrils. Model *A* in fact shows a 2.7 nm blue-shift (to 487.3 nm) relative to the Boltzmann-averaged absorption of water (490 nm). This is mainly due to the near-planar configuration of MHB bound this way as the dihedral angle scans showed similar wavelength shifts compared between $\varphi = 20°$ and $\varphi = 0°$. However, in the case of model *C* the optimal MHB conformation is unchanged, and we observe a 3.4 nm red-shift in the $S_0 \rightarrow S_1$ excitation wavelength. The red-shift for the model *C* is in qualitative agreement with the experimental data and suggests that the majority of MHB molecules are most likely bound with C+ approaching the sheet surface. Because of the lack of additional environmental contributions described above, the model *C* could not reproduce the magnitude of the experimental red-shift as accurately as in the case of implicit solvent models. However, a more exhaustive approach that models MHB binding and its spectral properties in the bound state by considering the statistical distribution of conformations of the dye bound on a larger sheet model with varied residues is currently beyond computational limits.

Table 1. Calculated and Experimental Shifts in Various Environments

	calc[a]		exp	
	$\lambda_{S_0 \rightarrow S_1}$ (nm)	$\Delta\lambda$[b]	$\lambda_{S_0 \rightarrow S_1}$ (nm)	$\Delta\lambda$[b]
vacuum	466			
water	490	0	604	0
ethanol	492	2	606	2
glycol/glycerol	502	10	614[c]	10
sheet model *C*[d] protein	493.4	3.4	623[e]	19
sheet model *A*[d] protein	487.3	−2.7		

[a] For the models in bulk solvent the wavelength of $S_0 \rightarrow S_1$ excitation is calculated considering the Boltzmann distribution of conformations obtained along the scan of φ torsional angle. Relative energies of the conformers were obtained at the B3LYP/6-31+G(d) level of theory. [b] The shift (in nm) relative to absorption peak obtained in water. [c] Wavelength maximum of MHB in 94% glycerol. [d] The sheet models with bound MHB were obtained with geometry optimization using ONIOM (ωB97X-D/6-31G(d):PM3). Excitation wavelength was calculated on the higher level layer at the B3LYP/6-31+G(d) level of theory with the IEFPCM model to include the effect of water. For more details on the model, see Figure S4. [e] Wavelength maximum of MHB bound to insulin fibrils.

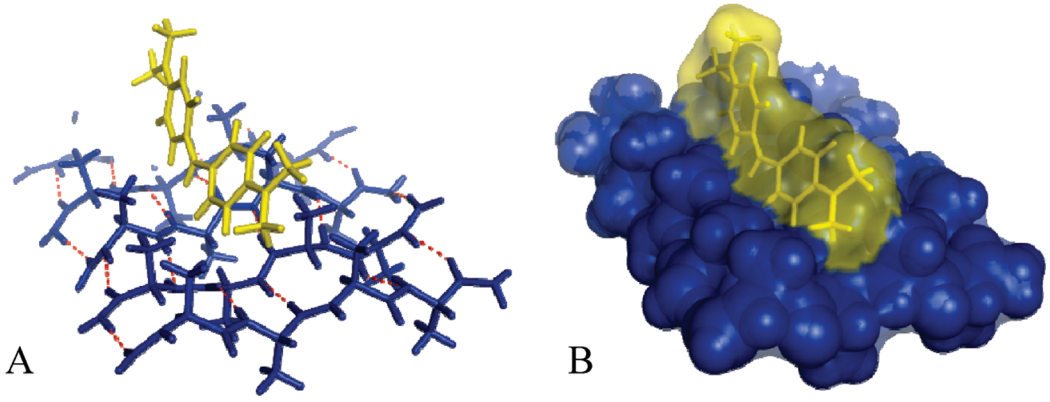

Figure 7. Sheet model *C*, having the C+ atom of MHB close to the sheet surface with bound MHB optimized using the ONIOM (ωB97XD/6-31G(d):PM3) approach. (A) The antiparallel sheet consisting of five peptide strands is shown by blue sticks, MHB is shown by yellow sticks, and hydrogen bonds between the peptide strands are marked by red dotted lines. The structure of MHB is close to its lowest energy conformation with $\varphi = -15.5°$ and $\varphi' = -11.5°$. (B) Surface model of the same sheet with the peptide strands shown by vdW spheres and MHB shown by sticks.

To validate the above model, the same sheet model was submitted to calculations using ThT instead of MHB. ThT was considered with two possible orientations; of the two orientations, one showed a small blue-shift while the other had a small red-shift in the absorption spectrum (for details see Supporting Information). This is similar to what was observed for MHB's orientation. To further compare the spectral changes of the two dyes, when changing to a more hydrophobic environment, we used an implicit solvent model calculations on both MHB and ThT. They both showed a 5.3 nm (ThT) and a 6.9 nm (MHB) red-shift when changing the environment from water to a more hydrophobic environment simulating a protein. Combined with the above sheet model calculations, these results confirm that the theoretical results correlate with the experiments and also point out that the red-shifts observed upon dye binding to amyloid fibrils are most likely due to the more hydrophobic protein environment.

In conclusion, we have shown that MHB is an excellent candidate for use as an amyloid fibril stain. MHB has shown to have a greater spectral sensitivity to changes in the protein environment than the widely used amyloid probe, ThT. The photophysical properties of MHB demonstrate a sensitivity to polarity along with an increased quantum yield when the rotation of one of its phenyl rings is restricted either due to confinement upon binding or due to high viscosity. The LD spectra and excitation spectra of MHB bound to insulin fibrils and MHB bound to lysozyme fibrils yield a more red-shifted peak for the MHB bound to insulin fibrils. This observation shows that MHB can give additional information about the environment or amyloid fibrils formed from different proteins.

Finally, it was shown through LD and molecular modeling that MHB aligns itself preferentially parallel with the amyloid fiber at an angle of 14°−22° to the fibril axis and along the grooves of the β-sheet, similar to ThT. As a result of this study, we have shown that another class of dye molecules, MHB, can be used as an additional biological marker for amyloid fibril detection. And we have shown that MHB is a better alternative to ThT and CR for spectroscopic studies due to its sensitivity to different environments and its ability to differentiate between different amyloid fibrils.

■ ASSOCIATED CONTENT

Supporting Information. A detailed description of how the *S* factor was calculated using a nonempirical method, the extended table of quantum mechanically computed spectral shifts in various environments using different levels of theory, MHB's HOMO and LUMO orbitals as a function of dihedral angle, and original sheet models of MHB and ThT bound calculated using ONIOM level of theory. This material is available free of charge via the Internet at http://pubs.acs.org.

■ AUTHOR INFORMATION

Corresponding Author

*Tel: +46.31.772.3856. Fax: +46.31.772.3858. E-mail: kitts@chalmers.se.

Funding Sources

B.N. was supported by grants from KAUST. C.C.K. and T.B.-S. both hold a KAUST postdoctoral fellowship.

■ ACKNOWLEDGMENT

King Abdullah University of Science and Technology (KAUST) (Grant KUK-11-008-23) is gratefully acknowledged. Special thanks to Johan Johansson for assessing the purity of the Michler's hydrol blue sample used in these experiments and to Maria Abrahamsson for help collecting the fluorescence lifetime data. We also thank Per Lincoln for stimulating discussions.

■ ABBREVIATIONS

MHB, Michler's hydrol blue; ThT, thioflavin T; TDDFT, time-dependent density functional theory; LD, linear dichroism; CR, Congo Red; LE, locally excited; TICT, twisted internal charge transfer; IEFPCM, integral equation formalism polarizable continuum solvent model; LD^r, reduced linear dichroism.

■ REFERENCES

(1) Chiti, F., and Dobson, C. M. (2006) Protein misfolding, functional amyloid, and human disease. *Annu. Rev. Biochem. 75*, 333–366.

(2) Dobson, C. M. (2003) Protein folding and misfolding. *Nature 426*, 884–890.

(3) Selkoe, D. J. (2003) Folding proteins in fatal ways. *Nature 426*, 900–904.

(4) Harper, J. D., and Lansbury, P. T. J. (1997) Models of amyloid seeding in Alzheimer's disease and Scrapie: Mechanistic truths and physiological consequences of the time-dependent solubility of amyloid proteins. *Annu. Rev. Biochem. 66*, 385–407.

(5) Murphy, R. M. (2002) Peptide Aggregation in Neurodegenerative disease. *Annu. Rev. Biochem. 4*, 155–174.

(6) Allsop, D., Swanson, L., Moore, S., Davies, Y., York, A., El-Agnaf, O. M. A., and Soutar, I. (2001) Fluorescence anisotropy: A method for early detection of Alzheimer B-peptide (AB) aggregation. *Biochem. Biophys. Res. Commun. 285*, 58–63.

(7) Fandrich, M., and Dobson, C. M. (2002) The behavior of polyamino acids reveals an inverse side chain effect in amyloid structure formation. *EMBO J. 21*, 5682–2690.

(8) Sipe, J. D. (1992) Amyloidosis. *Annu. Rev. Biochem. 61*, 947–975.

(9) Zeronvnik, E. (2002) Amyloid-fibril formation. *Eur. J. Biochem. 269*, 3362–3371.

(10) Sunde, M., Serpell, L. C., Bartlam, M., Fraser, P. E., Pepys, M. B., and Blake, C. C. F. (1997) Common core structure of amyloid fibrils by synchrotron X-ray diffraction. *J. Mol. Biol. 273*, 729–739.

(11) Makin, O. S., and Serpell, L. C. (2005) Structures for amyloid fibrils. *FEBS J. 272*, 5950–5961.

(12) Jimenez, J. L., Nettleton, E. J., Bouchard, M., Robinson, C. V., Dobson, C. M., and Saibil, H. R. (2002) The protofilament structure of insulin amyloid fibrils. *Proc. Natl. Acad. Sci. U.S.A. 99*, 9196–9201.

(13) Krebs, M. R. H., Bromley, E. H. C., and Donald, A. M. (2005) The binding of thioflavin-T to amyloid fibrils: localisation. *J. Struct. Biol. 149*, 30–37.

(14) Khurana, R., Ionescu-Zanetti, C., Pope, M., Li, J., Nielson, L., Ramirez-Alvarado, M., Regan, L., Fink, A. L., and Carter, S. A. (2003) A general model of amyloid fibril assembly based on morphological studies using atomic force microscopy. *Biophys. J. 85*, 1135–1144.

(15) Hwang, W., Zhang, S. G., Kamm, R. D., and Karplus, M. (2004) Kinetic control of dimer structure formation in amyloid fibrillogenesis. *Proc. Natl. Acad. Sci. U.S.A. 101*, 12916–12921.

(16) Lindgren, M., Sorgjerd, K., and Hammarstrom, P. (2005) Detection and Characterization of Aggregates, Prefibrillar Amyloidgenic Oligomers, and Protofibrils Using Fluorescence Spectroscopy. *Biophys. J. 88*, 4200–4212.

(17) Murali, J., and Jayakumar, R. (2005) Spectroscopic studies on native and protofibrillar insulin. *J. Struct. Biol. 150*, 180–189.

(18) Ban, T., Morigaki, K., Yagi, H., Kawasaki, T., Kobayashi, A., Yuba, S., Naiki, H., and Goto, Y. (2006) Real-time and single fibril

observation of the formation of amyloid B spherulitic structures. *J. Biol. Chem. 281*, 33677–33683.

(19) Ha, C., and Park, C. B. (2005) Template-Directed Self-Assembly and Growth of Insulin Amyloid Fibrils. *Biotechnol. Bioeng. 90*, 848–855.

(20) Kad, N. M., Myers, S. L., Smith, D. P., Smith, D. A., Radford, S. E., and Thomson, N. H. (2003) Hierarchical assembly of B_2-microglobulin amyloid *in vitro* revealed by atomic force microscopy. *J. Mol. Biol. 330*, 785–797.

(21) Bouchard, M., Zurdo, J., Nettleton, E. J., Dobson, C. M., and Robinson, C. V. (2000) Formation of insulin amyloid fibrils followed by FTIR simultaneously with CD and electron microscopy. *Protein Sci. 9*, 1960–1967.

(22) LeVine, H., III (2005) Multiple ligand binding sites on Aβ(1−40) fibrils. *Amyloid 12*, 5–14.

(23) Klunk, W. E., Jacob, R. F., and Mason, R. P. (1999) Quanitfying amyloid by Congo red spectral shift assay. *Methods Enzymol. 309*, 285–305.

(24) Benditt, E. P., Eriksen, N., and Berglund, C. (1970) Congo Red Dichroism with Dispersed Amyloid Fibrils an Extrinsic Cotton Effect. *Proc. Natl. Acad. Sci. U.S.A. 66*, 1044–1051.

(25) Jin, L.-W., Claborn, K. A., Kurimoto, M., Geday, M. A., Maezawa, I., Sohraby, F., Estrada, M., Kaminsky, W., and Kahr, B. (2003) Imaging linear birefringence and dichroism in cerebral amyloid pathologies. *Proc. Natl. Acad. Sci. U.S.A. 100*, 15294–15298.

(26) Khurana, R., Uversky, V. N., Nielson, L., and Fink, A. L. (2001) Is Congo Red an Amyloid Specific Dye? *J. Biol. Chem. 276*, 22715–22721.

(27) Klunk, W. E., Debnath, M. L., and Pettegrew, J. W. (1994) Development of small molecule probes for the beta-amyloid protein of Alzheimer's Disease. *Neurobiol. Aging 15*, 691–698.

(28) Turnell, W. G., and Finch, J. T. (1992) Binding of the Dye Congo Red to the Amyloid Protein Pig Insulin Reveals a Novel Homology Amongst Amyloid-Forming Peptide Sequences. *J. Mol. Biol. 227*, 1205–1223.

(29) Levine, H. (1999) Quantification of beta-sheet amyloid fibril structures with thioflavin T. *Method Enzymol. 309*, 274–284.

(30) LeVine, H., III (1993) Thioflavin T interaction with synthetic Alzheimer's disease β-amyloid peptides: Detection of amyloid aggregation in solution. *Protein Sci. 2*, 404–410.

(31) Maskevich, A. A., Sisiapura, V. I., Kuzmitsky, V. A., Kuznetsova, I. M., Povarova, O. I., Uversky, V. N., and Turoverov, K. K. (2007) Spectral properties of Thioflavin T in Solvents with Different Dielectic Properties and in a Fibril-Incorporated Form. *J. Proteome Res. 6*, 1392–1401.

(32) Nielson, L., Frokjaer, S., Brange, J., Uversky, V. N., and Fink, A. L. (2001) Probing the mechanism of insulin fibril formation with insulin mutants. *Biochemistry 40*, 8397–8409.

(33) Nielson, L., Khurana, R., Coats, A., Frokjaer, S., Brange, J., Vyas, S., Uversky, V. N., and Fink, A. L. (2001) Effect of environmental factors on the kinetics of insulin fibril formation: Elucidation of the molecular mechanism. *Biochemistry 40*, 6036–6046.

(34) Stsiapura, V. I., Maskevich, A. A., Kuzmitsky, V. A., Uverskii, V. N., Kuznetsova, I. M., and Turoverov, K. K. (2008) Thioflavin T as a Molecular Rotor: Fluorescent Properties of Thioflavin T in Solvents with Different Viscosity. *J. Phys. Chem. B 112*, 15893–15902.

(35) Voropai, E. S., Samtsov, M. P., Kaplevskii, K. N., Maskevich, A. A., Stepuro, V. I., Povarova, O. I., Kuznetsova, I. M., Turoverov, K. K., Fink, A. L., and Uverskii, V. N. (2003) Spectral properties of Thioflavin T and its complexes with amyloid fibrils. *J. Appl. Spectrosc. 70*, 868–874.

(36) Stsiapura, V., Maskevich, A. A., Kuzmitsky, V. A., Turoverov, K. K., and Kuznetsova, I. M. (2007) Computational Study of Thioflavin T Torsional Relaxation in the Excited States. *J. Phys. Chem. A 111*, 4829–4835.

(37) Singh, P. K., Kumbhakar, M., Pal, H., and Nath, S. (2010) Viscosity Effect on the Ultrafast Bond Twisting Dynamics in an Amyloid Fibril Sensor: Thioflavin-T. *J. Phys. Chem. B 114*, 5920–5927.

(38) Singh, P. K., Kumbhakar, M., Pal, H., and Nath, S. (2010) Ultrafast Bond Twisting Dynamics in Amyloid Fibril Sensor. *J. Phys. Chem. B 114*, 2541–2546.

(39) Stsiapura, V. I., Maskevich, A. A., Tikhomirov, S. A., and Buganov, O. V. (2010) Charge Transfer Process Determines Ultrafast Excited State Deactivation of Thioflavin T in Low-Viscosity Solvents. *J. Phys. Chem. A 114*, 8345–8350.

(40) Sulatskaya, A. I., Maskevich, A. A., Kuznetsova, I. M., Uversky, V. N., and Turoverov, K. K. (2010) Fluorescence Quantum Yield of Thioflavin T in Rigid Isotropic Solution and Incorporated into the Amyloid Fibrils, *Plos One 5*.

(41) Lakowicz, J. R. (2006) *Principles of Fluorescence Spectroscopy*, 3rd ed., Springer, Berlin.

(42) Momicchioli, F., Baraldi, I., Carnevali, A., Caselli, M., and Ponterini, G. (1993) Concerning medium polarity effects on the photophysics and photochemistry of TICT-forming dyes. *Coord. Chem. Rev. 125*, 301–316.

(43) Haidekker, M. A., Brady, T. P., Lichlyter, D., and Theodorakis, E. A. (2005) Effects of solvent polarity and solvent viscosity on the fluorescent properties of molecular rotors and related probes. *Bioorg. Chem. 33*, 415–425.

(44) Haidekker, M. A., and Theodorakis, E. A. (2007) Molecular rotors - fluorescent biosensors for viscosity and flow. *Org. Biomol. Chem. 5*, 1669–1678.

(45) Baraldi, I., Carnevali, A., Momicchioli, F., and Ponterini, G. (1992) Theoretical and experimental study of the electronic spectrum and photophysics of Michler's hydrol blue. *Chem. Phys. 160*, 85–96.

(46) Dapprich, S., Komaromi, I., Byun, K. S., Morokuma, K., and Frisch, M. J. (1999) A new ONIOM implementation in Gaussian98. Part I. The calculation of energies, gradients, vibrational frequencies and electric field derivatives. *J. Mol. Struct. 462*, 1–21.

(47) Norden, B., Elvingson, C., Eriksson, T., Kubista, M., Sjoberg, B., Takahashi, M., and Mortensen, K. (1990) Structure of a RecA-DNA Complex from Linear Dichroism and Small-Angle Neutron-Scattering in Flow-Oriented Solution. *J. Mol. Biol. 216*, 223–228.

(48) Tuite, E., Sehlstedt, U., Hagmar, P., Norden, B., and Takahashi, M. (1997) Effects of minor and major groove-binding drugs and intercalators on the DNA association of minor groove-binding proteins RecA and deoxyribonuclease I detected by flow linear dichroism. *Eur. J. Biochem. 243*, 482–492.

(49) Adachi, R., Yamaguchi, K., Yagi, H., Sakurai, K., Naiki, H., and Goto, Y. (2007) Flow-induced alignment of amyloid protofilaments revealed by linear dichroism. *J. Biol. Chem. 282*, 8978–8983.

(50) Bulheller, B. M., Rodger, A., Hicks, M. R., Dafforn, T. R., Serpell, L. C., Marshall, K. E., Bromley, E. H. C., King, P. J. S., Channon, K. J., Woolfson, D. N., and Hirst, J. D. (2009) Flow Linear Dichroism of Some Prototypical Proteins. *J. Am. Chem. Soc. 131*, 13305–13314.

(51) Dafforn, T. R., Rajendra, J., Halsall, D. J., Serpell, L. C., and Rodger, A. (2004) Protein fiber linear dichroism for structure determination and kinetics in a low-volume, low-wavelength couette flow cell. *Biophys. J. 86*, 404–410.

(52) Bengtsson, G. (1969) Polarographic Studies of Basic Triarylmethane dyes 0.4. Polarographic Behaviour of 2-thiophene Green P-Methoxy Malachite Green and Crystal Violet in Aqueous Solutions. *Acta Chem. Scand. 23*, 435–447.

(53) Frisch, M. J., Trucks, G. W., Schlegel, H. B., Scuseria, G. E., Robb, M. A., Cheeseman, J. R., Scalmani, G., Barone, V., Mennucci, B., Petersson, G. A., Nakatsuji, H., Caricato, M., Li, X., Hratchian, H. P., Izmaylov, A. F., Bloino, J., Zheng, G., Sonnenberg, J. L., Hada, M., Ehara, M., Toyota, K., Fukuda, R., Hasegawa, J., Ishida, M., Nakajima, T., Honda, Y., Kitao, O., Nakai, H., Vreven, T., Montgomery Jr., J. A., Peralta, J. E., Ogliaro, F., Bearpark, M., Heyd, J. J., Brothers, E., Kudin, K. N., Staroverov, V. N., Kobayashi, R., Normand, J., Raghavachari, K., Rendell, A., C, B. J., Iyengar, S. S., Tomasi, J., Cossi, M., Rega, N., Millam, J. M., Klene, M., Knox, J. E., Cross, J. B., Bakken, V., Adamo, C., Jaramillo, J., Gomperts, R., Stratmann, R. E., Yazyev, O., Austin, A. J., Cammi, R., Pomelli, C., Ochterski, J. W., Martin, R. L., Morokuma, K., Zakrzewski, V. G., Voth, G. A., Salvador, P., Danneberg, J. J., Dapprich,

S., Daniels, A. D., Farkas, O., Foresman, J. B., Ortiz, J. V., Cioslowski, J., and Fox, D. J. (2009) Gaussian 09, Revision A.02 ed., Gaussian, Inc., Wallingford, CT.

(54) Jacquemin, D., Perpete, E. A., Ciofini, I., and Adamo, C. (2009) Accurate Simulation of Optical Properties in Dyes. *Acc. Chem. Res. 42*, 326–334.

(55) Fabian, J. (2010) TDDFT-calculations of Vis/NIR absorbing compounds. *Dyes Pigments 84*, 36–53.

(56) Becke, A. D. (1993) Density-Functional Thermochemistry 0.3. The Role of Exact Exchange. *J. Chem. Phys. 98*, 5648–5652.

(57) Lee, C. T., Yang, W. T., and Parr, R. G. (1988) Development of the Colle-Salvetti Correlation-Engery Formula into a Functional of the Electron-Density. *Phys. Rev. B 37*, 785–789.

(58) Fabian, J. (2001) Electronic excitation of sulfur-organic compounds - performance of time-dependent density functional theory. *Theor. Chem. Acc. 106*, 199–217.

(59) Schreiber, M., Buss, V., and Fulscher, M. P. (2001) The electronic spectra of symmetric cyanine dyes: A CASPT2 study. *Phys. Chem. Chem. Phys. 3*, 3906–3912.

(60) Cances, E., Mennucci, B., and Tomasi, J. (1997) A new integral equation formalism for the polarizable continuum model: Theoretical background and applications to isotropic and anisotropic dielectrics. *J. Chem. Phys. 107*, 3032–3041.

(61) Perczel, A., Gaspari, Z., and Csizmadia, I. G. (2005) Structure and stability of beta-pleated sheets. *J. Comput. Chem. 26*, 1155–1168.

(62) Biancalana, M., and Koide, S. (2010) Molecular mechanism of Thioflavin-T binding to amyloid fibrils. *Biochim. Biophys. Acta, Proteins Proteomics 1804*, 1405–1412.

(63) Rodriguez-Rodriguez, C., Rimola, A., Rodriguez-Santiago, L., Ugliengo, P., Alvarez-Larena, A., Gutierrez-de-Teran, H., Sodupe, M., and Gonzalez-Duarte, P. (2010) Crystal structure of thioflavin-T and its binding to amyloid fibrils: insights at the molecular level. *Chem. Commun. 46*, 1156–1158.

(64) Goerigk, L., and Grimme, S. (2010) Assessment of TD-DFT methods and of various spin scaled CIS(D) and CC2 versions for the treatment of low-lying valence excitations of large organic dyes. *J. Chem. Phys.* 132.

(65) Goerigk, L., Moellmann, J., and Grimme, S. (2009) Computation of accurate excitation energies for large organic molecules with double-hybrid density functionals. *Phys. Chem. Chem. Phys. 11*, 4611–4620.

(66) Norden, B., Kubista, M., and Kurucsev, T. (1992) Linear Dichroism Spectroscopy of Nucleic Acids. *Q. Rev. Biophys. 25*, 51–170.

(67) Kitts, C. C., and Vanden Bout, D. A. (2009) Near-field scanning optical microscopy of fluorescent molecular probes binding to insulin amyloid fibrils. *J. Phys. Chem. B 113*, 12090–12095.

(68) Chai, J. D., and Head-Gordon, M. (2008) Long-range corrected hybrid density functionals with damped atom-atom dispersion corrections. *Phys. Chem. Chem. Phys. 10*, 6615–6620.